Paper No.
5933

NACE INTERNATIONAL CORROSION 2015 CONFERENCE & EXPO

MECHANISTIC STUDY OF THE EFFECT OF IRON SULFIDE LAYERS ON HYDROGEN SULFIDE CORROSION OF CARBON STEEL

Yougui Zheng, Jing Ning, Bruce Brown, David Young, Srdjan Nesic
Institute for Corrosion and Multiphase Technology
Department of Chemical and Biomolecular Engineering
Ohio University
342 W. State St.
Athens, OH 45701

ABSTRACT

A novel experimental set-up was designed and built to investigate the effect of iron sulfide layer growth on H_2S corrosion of carbon steel. Tests were conducted by purging 10% H_2S/N_2 into 1 wt.% NaCl solution at different temperature (25 °C-80 °C), different pH (pH 4 to pH 6) and different flow conditions (60 rpm and 600 rpm magnetic stirring rates). The exposure period was from 1 day to 7 days. The corrosion behavior was monitored by linear polarization resistance (LPR) and checked with weight loss analysis. The morphology and compositions of surface corrosion products were analyzed by Scanning Electron Microscopy (SEM/EDS), cross section analysis and X-ray Diffraction (XRD) methodology. The results show the balance between iron sulfide precipitation and undermining process, characterized by the scaling tendency, can lead to a variety of corrosion outcomes depending on the environmental parameters such as temperature, pH, and flow rate. Protective corrosion product layer and low corrosion rate were observed at high pH, temperature and low flow rate due to precipitation of a dense corrosion product layer.

Key words: carbon steel, hydrogen sulfide, iron sulfide, experiment, model.

INTRODUCTION

In the authors' previous work[1,2], an electrochemical model of H_2S corrosion without iron sulfide layer growth has been developed to address the initial stages of the corrosion process, avoiding the complex issues associated with formation and growth of an iron sulfide layer. However, long term H_2S corrosion experienced in lab or field conditions is dominated by the formation of the iron sulfide corrosion product layer. The corrosion product layer can be very protective, but there are also some reports of localized

corrosion related to iron sulfide corrosion products failures. The magnitude of the corrosion attack is apparently very dependent on the nature of the iron sulfide corrosion product layer[3]. The protective layer is usually dense and has a good adherence to the steel surface. The less protective layer is usually porous, flaky, and non-adherent to the steel surface and may lead to localized corrosion and failures.

The mechanism of H_2S corrosion of carbon steel under corrosion product layer forming conditions is a complex process that still lacks a comprehensive understanding. A few years ago, a predictive model for H_2S corrosion was developed by Sun and Nesic[4,5], who proposed an inner 1-10 nm thin inner mackinawite film acting as a solid state diffusion barrier and a porous outer iron sulfide layer formed by spalling of the inner iron sulfide film. Due to the presence of these two layers, the corrosion rate is always under mass-transfer control, as Sun *et al.*[4] hypothesized. The proposal that two different iron sulfide layers form on the steel surface, which is the key for understanding H_2S corrosion, is accepted in the corrosion community. However, the mechanism of the formation of the two layers is still under debate.

A somewhat similar alternative hypothesis is proposed by the authors in the present work, but one that is better defined and more thoroughly verified by experimental results. It can be summarized as follows: a very thin inner iron sulfide film of mackinawite is first formed *via* a chemisorption process, *i.e.*, by a direct reaction of exposed surfaces of Fe with dissolved H_2S.[6] This film forms rapidly and its presence can be determined, based on the thermodynamic arguments for chemically adsorbed species; see the appropriate stability diagrams developed by Marcus, *et al.*[7]. The thicker outer layer of iron sulfide is formed by precipitation on the initially chemisorbed film of mackinawite, which is a preferred nucleation site. The formation of this outer layer depends on the thermodynamic stability for iron sulfide at the steel surface, i.e. on the surface water chemistry.[8] This layer may end up being dense and protective or porous and non-protective depending on the competition between precipitation (which favors protection) and corrosion (which undermines it). In the current study, the objective was to verify this new hypothesis about the mechanism of formation and the role of iron sulfide corrosion product layers in H_2S corrosion.

EXPERIMENTAL METHOD

Equipment

In the literature, many corrosion experiments have been conducted in closed systems (e.g. autoclaves) with a limited inventory of fluids. In that scenario, the aqueous Fe^{2+} concentration and pH may increase significantly with exposure time and affect the iron sulfide layer formation and corrosion rates. Therefore, a new approach with continuous replenishment of fluid was developed to investigate the effect of iron sulfide layer on corrosion under stable environmental conditions. The experiment apparatus is shown in Figure 1. The system consists of four main components: the pre-conditioning vessel, the test cell (shown in more detail in Figure 2), the gas scrubber, and the chemical scrubber.

The pre-conditioning vessel holds up to 20 L of a N_2 purged aqueous solution and is equipped with four ports: gas inlet, gas outlet, a port for pH probe and the replenishment of solution and an outlet port connecting to a line going to the gear pump. The pH of the solution in the pre-conditioning vessel was adjusted manually by adding a deoxygenated hydrochloric acid (HCl) or sodium hydroxide (NaOH) solution. The adjustment was made depending on the target water chemistry conditions in the test cell. The pump rate used for transferring the replenishment solution from the pre-conditioning vessel into the test cell depends on the pH drift of the solution in the test cell, which is related to corrosion rate. When the corrosion rate is high, Fe^{2+} release is faster and pH increases quickly, so the pump rate was set to a higher value (3-6 ml/min), and vice versa, when corrosion rate of the specimen in the test cell is low, pump rate was set to a lower value (1-2 ml/min). The pH of the solution in the test cell was continuously monitored and the pump rate is adjusted accordingly.

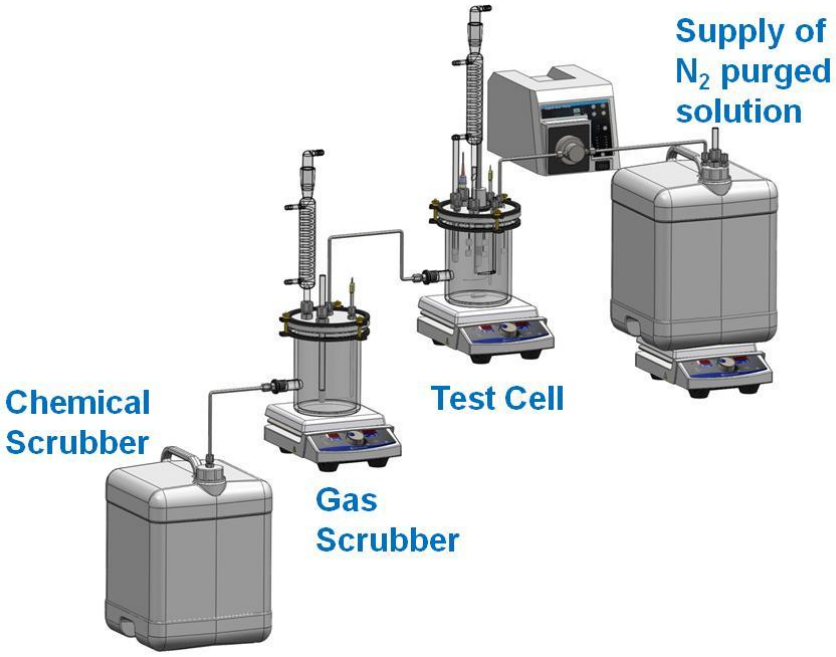

Figure 1. Schematic of the experimental set-up for long tern H_2S corrosion tests.

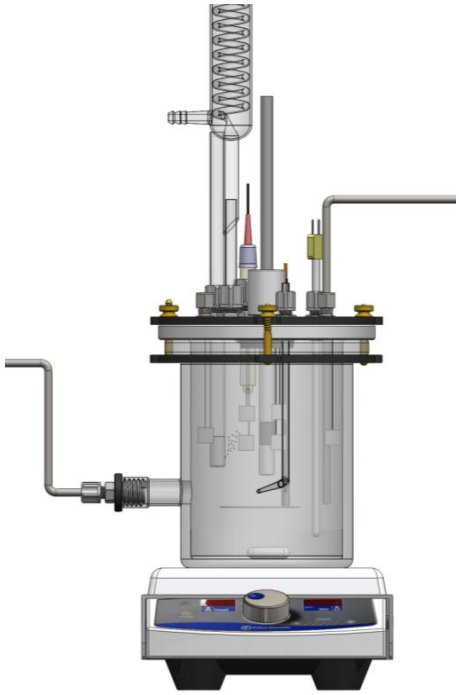

Figure 2. Schematic of the test cell for the long term H_2S corrosion test

The test cell is similar to the standard three electrode glass cell, as described in the authors' previous work[1]. The counter electrode was a platinum wire. The reference electrode was Ag/AgCl in saturated KCl

electrolyte. The working electrode was a cylindrical X-65 carbon steel specimen with *ca.* 5.4 cm^2 surface area. However, several improvements were made to address the specific research needs. First, in order to investigate the growth of iron sulfide layer, several square specimens (1.2cm×1.2cm×0.2cm, carbon steel) were hung from nylon string into the solution in the test cell. These were recovered for surface analysis and weight loss measurements after different exposure times.

A magnetic stirrer at the bottom was used to simulate flowing conditions instead of using a rotating cylinder electrode (RCE). The RCE can be inserted only as a single specimen, which is used for electrochemical measurement and is not as suitable for surface analysis and weight loss measurements. If any other specimens are placed in the solution along with the RCE they would reside in an almost stagnant solution, which is considerably different from the flow condition seen at the RCE. When a magnetic stirrer was used, the flow condition for all the specimens was similar. The effect of flow on iron sulfide layer growth and corrosion rate was investigated by using this experimental set-up.

Another new feature of this test cell was the addition of two extra ports: one port at the top for the inflow of fresh solution added from the pre-conditioning vessel and one side port at the bottom for the solution exiting to the gas scrubber. The solution level of the test cell was controlled by the U-shaped tube connected between the test cell and gas scrubber.

The gas scrubber (in the form of a glass cell) was used to collect the solution exiting from the test cell. N_2 gas was purged to remove dissolved H_2S. The addition of concentrated NaOH solution to the scrubbing liquid at the bottom was used to neutralize any leftover H_2S in the solution. The liquid water scrubber (a high volume container) was used to collect the solution out of the gas scrubber. Solid NaOH was also added to remove final traces of dissolved H_2S.

Material

Corrosion of API[(1)] 5L X65 pipeline steel was investigated. The composition of this type of steel is shown in Table **1**. One single cylindrical electrode (RCE) and multiple hanging specimens machined from the parent steel material were used. The RCE has a diameter of 1.20 cm and a working surface area of 5.4 cm^2. The hanging specimen dimensions are 1.2 cm×1.2 cm × 0.2 cm, with a surface area of around 3.8 cm^2.

Table 1. Chemical composition of the carbon steel used in RCE (wt%).

Cr	Mo	S	V	Si	C	Fe	Ni	Mn	P
0.14	0.16	0.009	0.047	0.26	0.13	Balance	0.36	1.16	0.009

Procedure

All experiments were performed in the test cell with the solution saturated with a H_2S/N_2 mixture at atmospheric pressure. The test cell can hold 2 L of 1 wt% NaCl electrolyte. Initially the solutions in both the test cell and the pre-conditioning cell were both purged with N_2 for at least three hours (often overnight), to remove dissolved oxygen. After the solution was deoxygenated, the designated H_2S/N_2 mixed gas was introduced to the solution in the test cell by purging for at least half an hour to saturate the electrolyte. The solution pH in both the test cell and pre-conditioning cell were adjusted to the set value by adding deoxygenated aqueous HCl or NaOH solution. Prior to immersion, the carbon steel specimen surfaces were polished with 400 and 600 grit silicon-carbide paper, rinsed with isopropyl alcohol and dried in air. Experimental conditions are summarized in Table 2.

[(1)]American Petroleum Institute(API), 1220 L Street, NW, Washington, DC 20005-4070

Table 2. Test matrix for studying the effect of iron sulfide layer on corrosion

Parameter	Description
Solution	1 wt.% NaCl
Temperature	25 °C, 80 °C
Total pressure	1 bar
Magnetic stirring rate	60, 600rpm
Initial pH	4.0, 5.0, 6.0
H_2S concentration	10% H_2S/N_2
Test duration	4-7 days

Corrosion rates for carbon steel were determined using both the electrochemical and weight loss techniques. During the test, linear polarization resistance (LPR) and electrochemical impedance spectroscopy (EIS) were used to monitor the corrosion rate. LPR measurements were conducted in a range of ±5 mV with respect to the open circuit potential (OCP) and a scan rate of 0.125 mV/s. EIS measurements were performed in the frequency range from 5 kHz to 3 mHz, with an alternating current (AC) signal amplitude of 10 mV(rms) at the OCP. Clarke solution[9] was used to remove the corrosion product layer from the specimens surface for weight loss corrosion rate calculation. After the experiments, the specimens were evaluated through additional *ex-situ* analyses. The morphology and compositions of corrosion products were analyzed using a scanning electron Microscope (SEM), energy dispersive X-ray spectroscopy (EDS), and X-ray diffraction (XRD).

RESULTS AND DISCUSSION

Formation of the Inner Thin Iron Sulfide Film and Its Effect on H_2S Corrosion

In the Introduction section, an argument was made that there is a thin inner iron sulfide layer on the steel surface. The existence of this layer was proposed by Sun *et al.* [3,4] who suggested that it forms by a 'solid state' reaction between iron and H_2S and that it reduces the corrosion rate by acting as a solid state diffusion barrier. However, we now believe that it is more likely that this thin inner layer forms by chemisorption and retards the corrosion rate by interfering with the kinetics of different electrochemical reactions. The evidence for this alternative proposal will be presented in the text below. There are two main independent arguments in favor of existence of this chemisorbed sulfide film.

First, the formation of the inner adsorbed sulfide film is not only found on an iron substrate, a similar adsorbed sulfide film is also observed on other metal substrates, such as platinum (Pt), gold (Au), nickel (Ni), and copper (Cu)[10]. Jiang and Carter[6,11] predicted HS^- can be strongly chemisorbed on the iron surface using density functional theory (DFT). Marcus [10] also confirmed that the dissolved H_2S species such as H_2S, HS^- can be specifically adsorbed on the metal surface and form a chemisorbed layer. The layer forms rapidly and its presence is dependent on the thermodynamic stability of the adsorbed sulfide layer on Fe or other substrates at the given conditions. An E-pH diagram is the most typical way to represent the thermodynamic stability of different species for a redox process. Marcus *et al.* [7] developed an E-pH diagram for sulfur species adsorbed on iron to predict the formation of this chemically adsorbed layer, as Figure 3 shows. The condition for this diagram is 25 °C, 10^{-4} mol/kg total S concentration and 10^{-4} mol/kg Fe^{2+} concentration. The red line at the bottom is the transition line between the H_2O adsorbed layer and sulfide adsorbed layer (sulfide adsorbed layer coverage $\theta_{S(ads)}$ = 0.99, H_2O adsorbed layer coverage $\theta_{H_2O(ads)}$ = 0.01). Above this red line, a surface coverage of the sulfide adsorbed layer is higher than 0.99 and H_2O coverage is less than 0.01, which means the sulfide adsorbed layer is stable. Vice versa, below this red line, the adsorbed sulfide layer is unstable. The area in the blue square represents

the range of potential (-0.3 to -0.6 V) and pH (2 to 7) for the common corrosion conditions for mild steel corroding in a H_2S saturated solution. Comparing this with the stability domain of the adsorbed sulfide layer in Figure 3 shows the sulfide layer is very stable at these conditions except for some very extreme conditions (low pH and low potential). It is also found that adsorbed sulfide film can exist under conditions in which no bulk iron sulfide (Mackinawite) is stable.

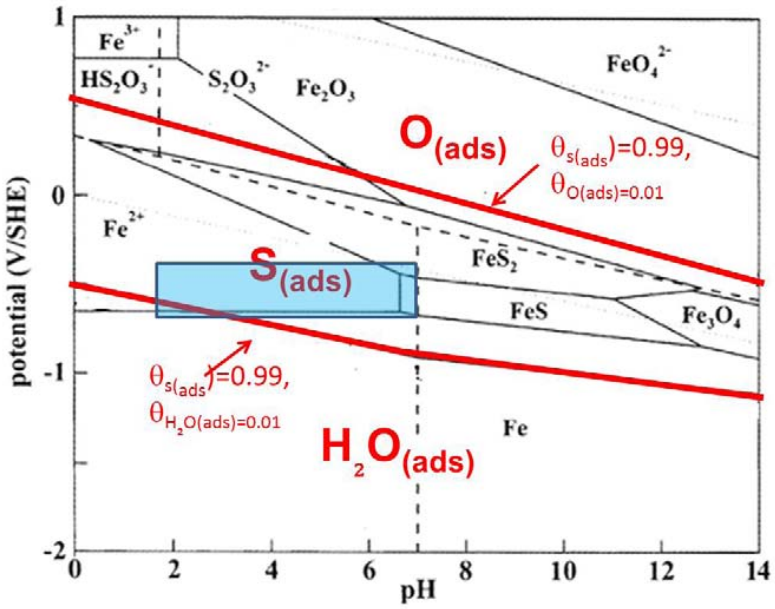

Figure 3. E-pH diagram for sulfur adsorbed on Fe (25°C, Total sulfur concentration= 10^{-4} mol/kg) (Reproduced with permission from Marcus and Protopopoff[7], Copyright ©1990, The Electrochemical Society).

Not only are the dissolved H_2S species easily adsorbed on an iron surface, but other sulfur containing species such $HS_2O_3^-$, $S_2O_3^{2-}$ and thiols (R-SH) can also be readily adsorbed on an iron surface. Comparison between H_2S and thiol adsorption is performed here. Similar adsorption binding energy has been observed for thiols[12] and aqueous H_2S[13] on an iron substrate. Volmer, *et al.*[14] and Lay *et al.*[15] have proposed the adsorption mechanism of thiols on a metal surface. The sulfur atoms in thiols are covalently bonded to the metal surface. The bond from chemisorption of a thiol to the metal surface can only be formed by cleavage of the S-H bond. This mechanism can be interpreted to be the same for aqueous H_2S, because H_2S can be thought of as the smallest of thiols, and an analogy between aqueous H_2S and thiol adsorption on mild steel can be accepted.

However, a question remains about how does this chemisorbed sulfide layer affect the electrochemical reactions in H_2S corrosion? It was previously proven that chemisorption of H_2S on the platinum can slow down the hydrogen evolution rate (HER)[16], which is the most important cathodic reaction in the corrosion process. As Figure 4 shows, the exchange current density of the hydrogen evolution rate (HER) on Pt decreases with an increase in surface coverage by sulfides. The sulfide coverage was measured by Auger spectroscopy, low energy electron diffraction (LEED), and ^{35}S radiotracer techniques. In addition, if an analogy between aqueous H_2S and thiol adsorption on mild steel can be accepted, the observations of the retardation effect due to thiol adsorption on electrochemical reactions can be taken as the evidence. Stratmann, *et al*.[17] have reported that, during thiol adsorption, the sulfide adsorbed layer was established within 10 s, yielding a film composed of domains with a lateral size of 10-20 nm. This adsorbed layer can cause a decrease of capacitance due to the pushing apart of the double layer, and affect the charge

transfer reaction. Volmer, *et al*.[12] stated that both propanethiol (C_3H_7SH) and decanethiol ($C_{10}H_{21}SH$) chemisorb onto iron and 10-nm-thick multilayer films can be identified, which show excellent blocking of oxygen reduction. Thiols or other sulfur containing compounds (such as thiosulfate), have been used as corrosion inhibitors for carbon steel corrosion.[18]

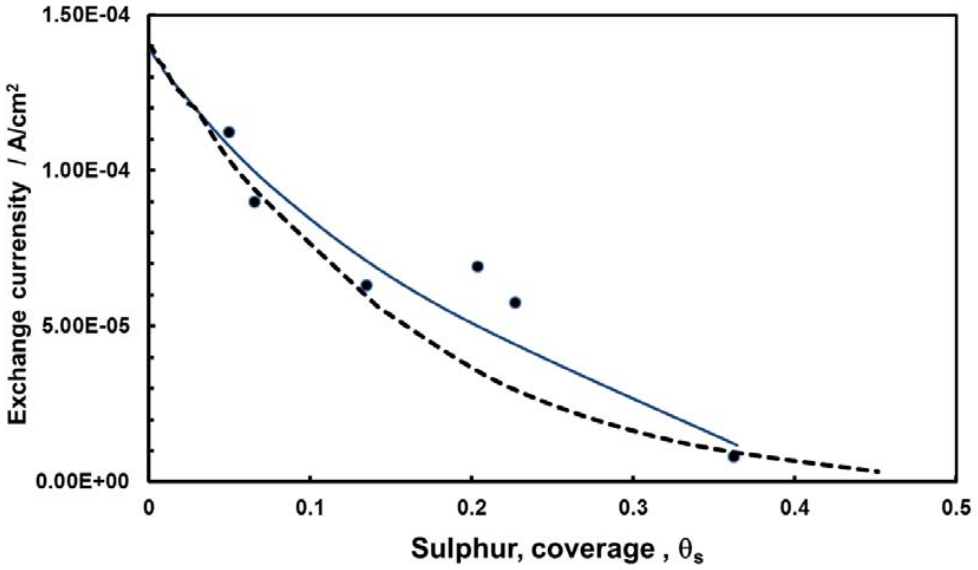

Figure 4. Exchange current density of HER on Pt (111) vs. the sulfur coverage. The curved dash line is calculated according to $i_0=i_{0(\theta s=0)}(1-\theta_s)$, with $i_{0(\theta s=0)} = 1.4\times10^{-4}$ A cm^{-2}. (Reproduced with permission from Marcus *et al.* [16], Copyright ©1987, American Vacuum Society).

Moreover, the retardation effect of the first sulfide layer on the charge transfer reactions, especially the anodic reaction and H_2O reduction is also observed in potentiodynamic sweeps as shown in the authors' previous work.[1,2] Figure 5 shows a comparison of potentiodynamic sweeps conducted in a H_2S saturated aqueous environment and a similar environment containing no H_2S.[1] The anodic reaction and the H_2O reduction current density are retarded with addition of H_2S. Actually a similar retardation effect on anodic reaction from HAc was also observed by Crolet *et al.*[19] , Sun *et al.*[20], and Gulbrandsen and Bilkova [21].

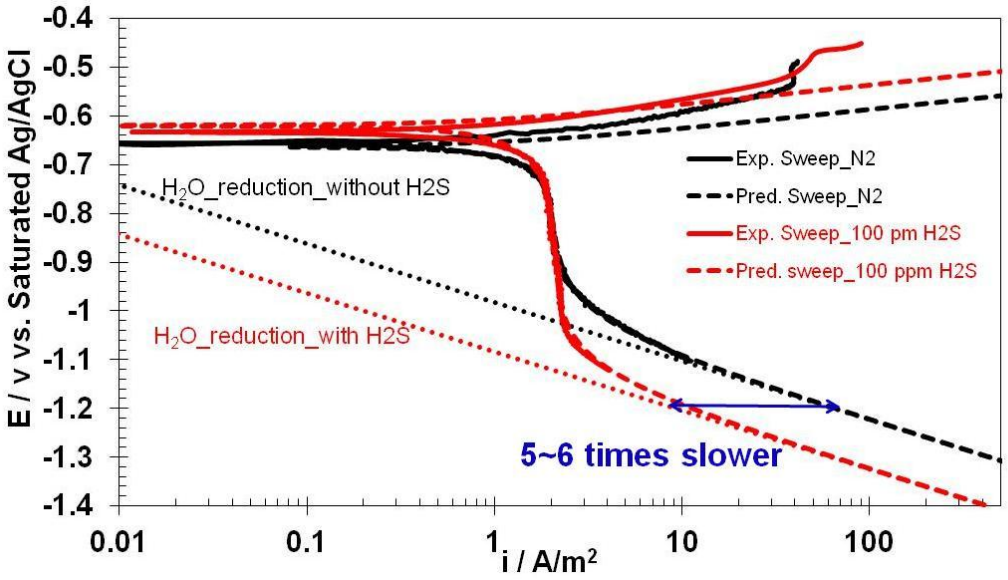

Figure 5. Comparison of potentiodynamic sweeps for H_2S environment and non-H_2S environments. (Reproduced with permission from Zheng *et al.*[1], Copyright ©2014, NACE International)

The mechanism of the retardation coming from adsorbed H_2S can be explained by the changes in the double layer. The thickness of the first inner sulfide film was reported[13] to be 10 nm, which is approaching the same order of magnitude as the double layer thickness (10-100 nm).[22] The typical double layer has adsorbed H_2O molecules at the metal/solution interface. The adsorption of sulfide species can be considered to be a competing or "replacement" reaction in which sulfide species replace H_2O molecules adsorbed at the metal/solution interface and affect the properties of the double layer.

In summary, the analysis above has confirmed that it is most likely that the very thin inner sulfide layer is formed by chemisorption. The chemically adsorbed sulfide layer can slow down the charge transfer reaction kinetics, where both anodic and cathodic reactions are affected. The previously developed electrochemical corrosion model by the present authors[1,2] already includes this influence on corrosion kinetics by reducing the charge transfer exchange current density.

Formation and Effect of the Outer Iron Sulfide Layer on Corrosion

As stated in the Introduction section, a much thicker outer iron sulfide layer may form, depending on the surface saturation value for iron sulfide, in relation to the precipitation reaction:

$$\mathrm{Fe}^{2+}_{(\mathrm{aq})} + \mathrm{S}^{2-}_{(aq)} \rightleftharpoons \mathrm{FeS(s)} \quad (1)$$

The saturation value for iron sulfide formation is calculated based on Equation (2).

$$\mathrm{S_{FeS}} = \frac{\mathrm{c_{Fe^{2+}} c_{S^{2-}}}}{\mathrm{K_{spFeS}}} \quad (2)$$

By knowing the concentration of Fe^{2+} and S^{2-} ions at the steel surface, the likelihood of formation of iron sulfide by precipitation can be determined. When $S_{FeS} > 1$, the multiple of the concentrations of Fe^{2+} and

S^{2-} ions exceeds the solubility limit, and iron sulfide may precipitate on the steel surface. When $S_{FeS} < 1$, iron sulfide cannot form and any existing iron sulfide may be dissolved from the steel surface. Importantly, not every type of precipitated iron sulfide layer is protective. The corrosion rate is directly related to the properties of the iron sulfide layer: its morphology, porosity and attachment to the corroding surface. Notably iron sulfide layer thickness is often a poor predictor of protectiveness. The easiest way to quantify the likelihood of obtaining a protective iron sulfide layer is via the surface scaling tendency (SST) which describes the relative rate of precipitation (formation) with respect to the corrosion rate (undermining rate) at the steel surface, expressed in the same units, as Equation (3) shows.

$$\mathrm{SST} = \frac{\text{Precipitation Rate (PR)}}{\text{Corrosion rate (CR)}} \tag{3}$$

When $\mathrm{SST} \geq 1$, the rate of iron sulfide precipitation (formation) at the steel surface equals or exceeds the rate of corrosion (undermining), and the condition is favorable for formation of dense, protective iron sulfide layers which can lead to corrosion rate reduction. *Vice versa* when $\mathrm{SST} < 1$, the corrosion process undermines the newly formed iron sulfide layer faster than precipitation can fill in the voids. A porous and non-protective iron sulfide layer forms, which can be very thick.

Three series of controlled corrosion tests in the presence of iron sulfide were designed in order to verify the hypothesis related mechanism of formation of the outer iron sulfide layer by precipitation which is different from the proposal of Sun *et al.*[4] based on spalling of the thin inner layer. The experiments were also meant to and check the validity of SST as an effective indicator of protective film formation in H_2S corrosion of mild steel.

Test series #1 is focused the effect of pH. As previously known, precipitation rates increase and corrosion rates decrease with increasing pH, so the SST will be higher. This is favorable for protective iron sulfide layer formation. Test series #2 is related to the effect of flow. Species transport in turbulent flow affects the surface concentration of species. Lower flow can cause the increase of surface ferrous ion concentration and pH[23], making the surface condition more favorable for iron sulfide precipitation due to an increased precipitation rate and higher SST. Test series #3 looked into the effect of temperature. Generally, increased temperature accelerates the precipitation kinetics more than it does the corrosion rate, making the SST higher which should aid the formation of a protective layer.

Test series #1 - pH Effect

Corrosion Behavior

Corrosion rates from LPR measurement at different pH values are shown in Figure 6. The pH has a strong influence on the corrosion rate. At pH 4.0, the increase of corrosion rate with time can be attributed to the presence of an iron carbide network exposed by corrosion. It has been reported that iron carbide can accelerate the corrosion rate due to the increase of the cathodic reaction area[24,25]. At pH 5.0 and pH 6.0, the decrease of corrosion rate is the result of the protective iron sulfide layer formed on the steel. It is also shown that the iron sulfide layer formed at pH 6.0 is more protective compared with that obtained at pH 5.0, due to the high SST at pH 6.0.

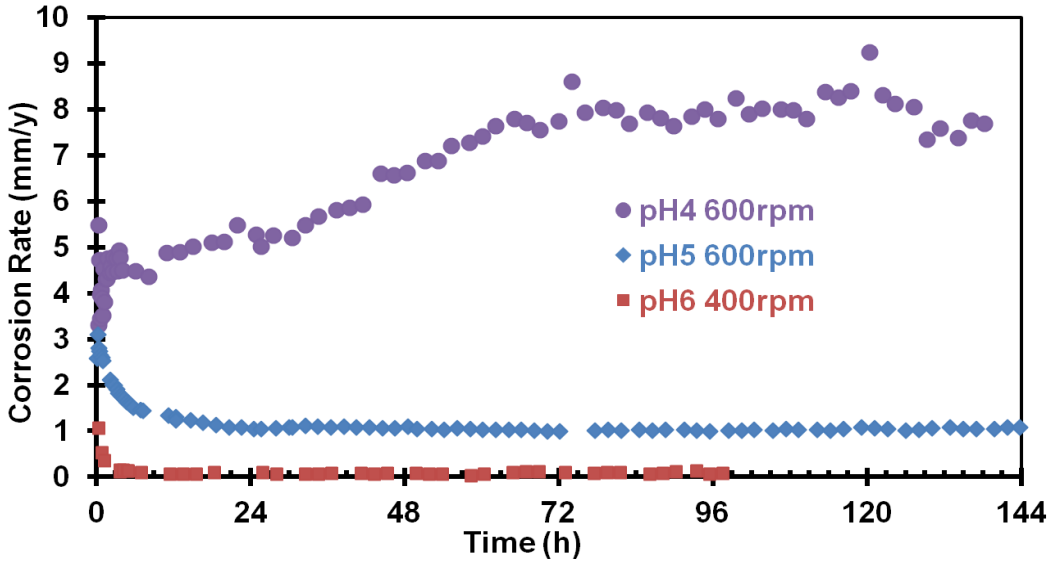

Figure 6. Corrosion rate with time at different pH, P_{total} = 1 bar, 10% H_2S/N_2 (0.05 bar H_2S), 80 °C.

Corrosion Product Layers

Figure 7 shows the surface morphology and cross section of the corrosion product layer as a function of pH after a one day exposure. Top view SEM images show that a surface layer had formed on all specimens after one day of corrosion.

At pH 4.0, the surface layer has a very open and porous structure, as shown in Figure 7 (a) and (d), so the product cannot provide any protection against corrosion. The layer thickness is about 4.5 µm, which is much smaller than the average of 10 µm of metal lost due to corrosion during the experiment. That is probably due to the layer being too loose and detached from the steel surface, so it could be easily removed by wall shear stress.

At pH 5.0, the top surface layer displayed a flaky structure. Parts of the layer had spalled off and revealed the presence of much smaller crystallites under the outer layer. From the cross section analysis, the corrosion product is also composed of two parts: a dense and adherent layer covering the steel surface with a thickness on average of about 5 µm and a second very porous layer on top. By comparison, the steel thickness loss due to corrosion is about 5 µm, which corresponds roughly to the thickness of the dense layer. It is most likely this layer is the result of the immediate precipitation of Fe^{2+} released from corrosion. The second porous layer has most likely formed through a slow precipitation from Fe^{2+} in the bulk solution. This second porous layer is not as well attached and corresponds to the flaky features observed in the top view SEM image.

At pH 6.0, the surface was mostly covered with a much denser layer. Similar to the specimen at pH 5.0, small crystals were observed on areas where the outer layer had spalled off. From the cross section image, a thin dense and seemingly adherent layer covers the steel surface with a thickness around 1 µm, which is close to the metal loss thickness by corrosion (0.7 µm).

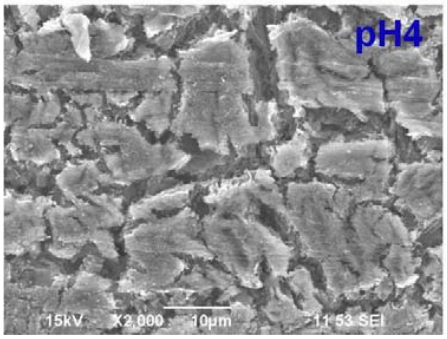

(a) SEM image of corrosion product layer at pH 4.0

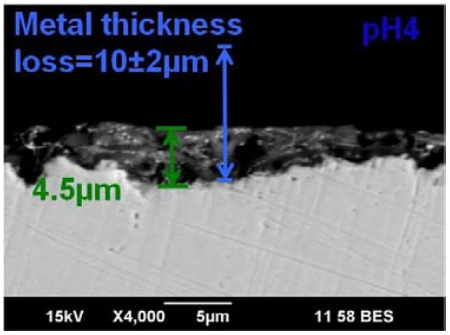

(d) Cross section of steel specimen with corrosion product layer at pH 4.0

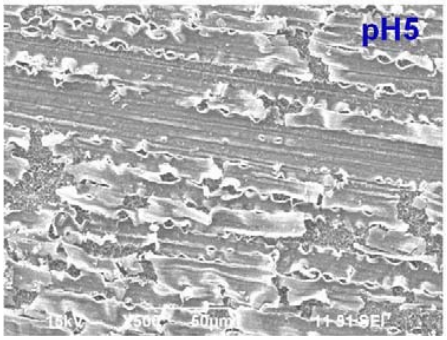

(b) SEM image of corrosion product layer at pH 5.0

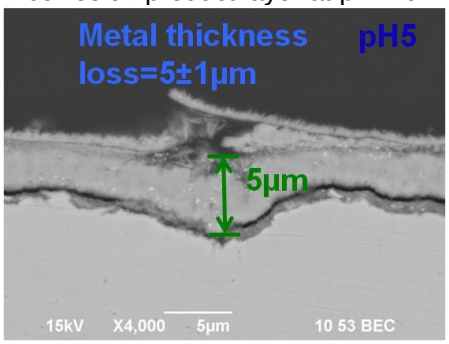

(e) Cross section of steel specimen with corrosion product layer at pH 5.0

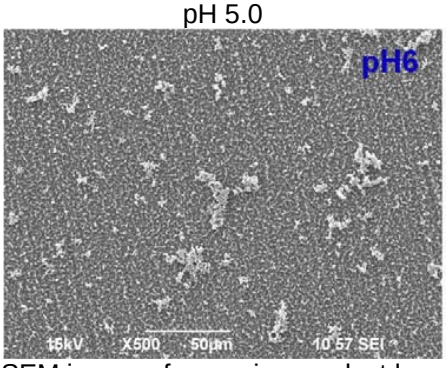

(c) SEM image of corrosion product layer at pH 6.0

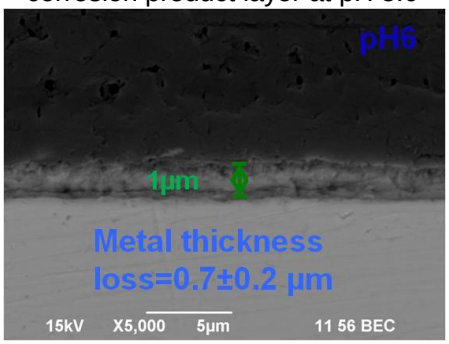

(f) Cross section of steel specimen with corrosion product layer at pH 6.0

Figure 7. SEM image and cross section of corrosion product layer at various pH conditions, P_{total} = 1 bar, 10% H_2S /N_2 (0.05 bar H_2S), 80 °C, duration 1 day.

The surface morphology of the corrosion product layer and cross section analysis at the end of tests are shown in Figure 8. The structure of the corrosion product layers present the same characteristics as were observed after one day of corrosion. That is the main cause of corrosion rates remaining the same from 1 day to the end of the tests at 6 days.

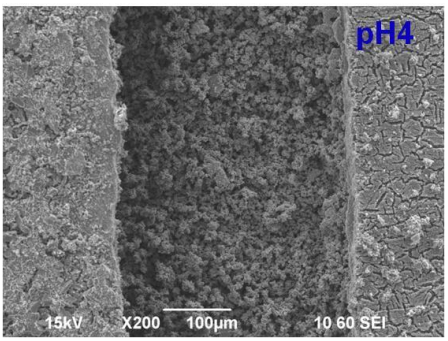

(a) SEM image of corrosion product layer at pH 4.0

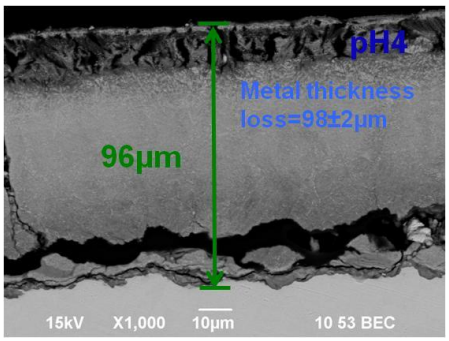

(d) Cross section of steel specimen with corrosion product layer at pH 4.0

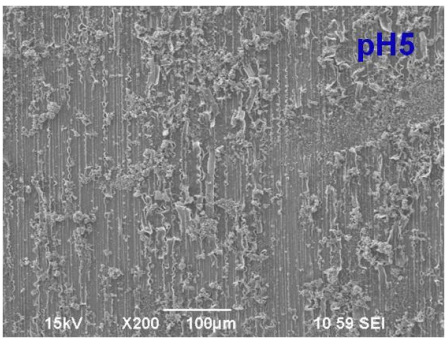

(b) SEM image of corrosion product layer at pH 5.0

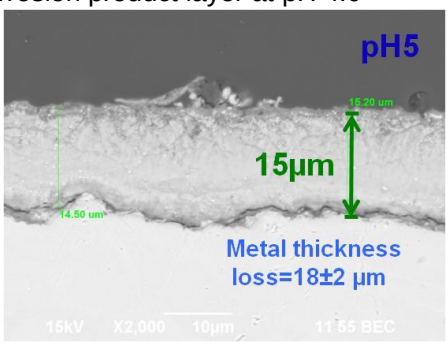

(e) Cross section of steel specimen with corrosion product layer at pH 5.0

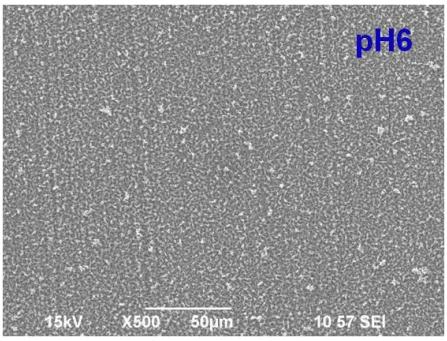

(c) SEM image of corrosion product layer at pH 6.0

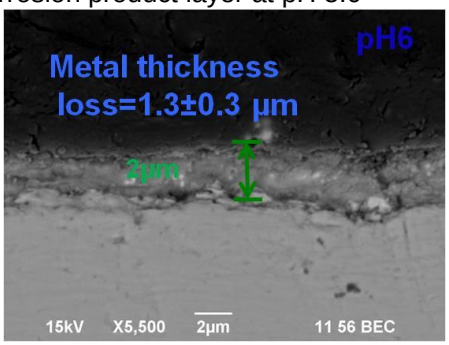

(f) Cross section of steel specimen with corrosion product layer at pH 6.0

Figure 8. SEM image and cross section of corrosion product layer at various pH conditions, P_{total} = 1 bar, 10% H_2S /N_2 (0.05 bar H_2S), 80 °C, 7 days exposure at pH 4.0 and pH 5.0, 4 days exposure at pH 6.0.

At pH 4.0, a thick, porous and very detached layer covers the steel surface, which does not provide any protective effect. At pH 6.0, a thin, dense and adherent layer is present on the steel surface, which is very protective against corrosion. The protectiveness of the iron sulfide layer at pH 5.0 is intermediate with respect to the layers at pH 4.0 and pH 6.0. The corrosion layer was somewhat protective, as the final steady-state corrosion rates were much lower than the initial corrosion (3.2 mm/y to 1.0 mm/y), but was still around 1 mm/y.

Moreover, the corrosion product layers at the end of the tests (4- 7 days) are much thicker than those after 1 day of corrosion, and appears to be very dense, but corrosion rates do not change much. This is indicative that the thickness of corrosion product layers and apparent porosity as seen in SEM images, play a negligible role in corrosion rate reduction. Lack of correlation of the overall layer thickness and associated corrosion rate has also been observed in CO_2 corrosion in the presence of iron carbonate

layers [26]. The corrosion rate is mostly likely related to the porosity and morphology of the thin corrosion product layer immediately adjacent to the steel surface (first few microns) and to how well it is attached to the steel surface, rather than the overall layer thickness and porosity.

Test series #2 - Flow Effect

Corrosion Behavior

Turbulent flow can affect the surface water chemistry by changing mass transfer rate of species moving from the bulk to the steel surface or *vice versa*. At low flow rate, the surface concentration for most of the species is different from bulk concentrations. The surface pH has been shown to be 1 to 2 units higher than the bulk solution pH [23,26]. When that happens and the surface pH is higher, the conditions are more favorable for iron sulfide formation on the steel surface as the precipitation rate will be higher, and the corrosion rate is lower; therefore the SST will be higher and the protective corrosion product layer is easier to form.

Figure 9 shows corrosion rates from LPR measurement at different flow rates at pH 4.0. At the higher flow rate (600 rpm stirring rate), corrosion rate increases with time, meaning that no protective layer formed on the steel surface. At the lower flow rate (60 rpm stirring rate), the corrosion rate reduces from 2.2 mm/y to about 1.5 mm/y, which is due to the formation of the somewhat protective layer on the surface. The bulk water chemistry is exactly the same in these two cases. The different roles of the corrosion product layer resulted from the difference in surface water chemistry caused by the turbulent mixing. The same effect was observed at pH 5.0 as shown in Figure 10. A lower flow rate was observed to be favorable for the protective corrosion product layer formation.

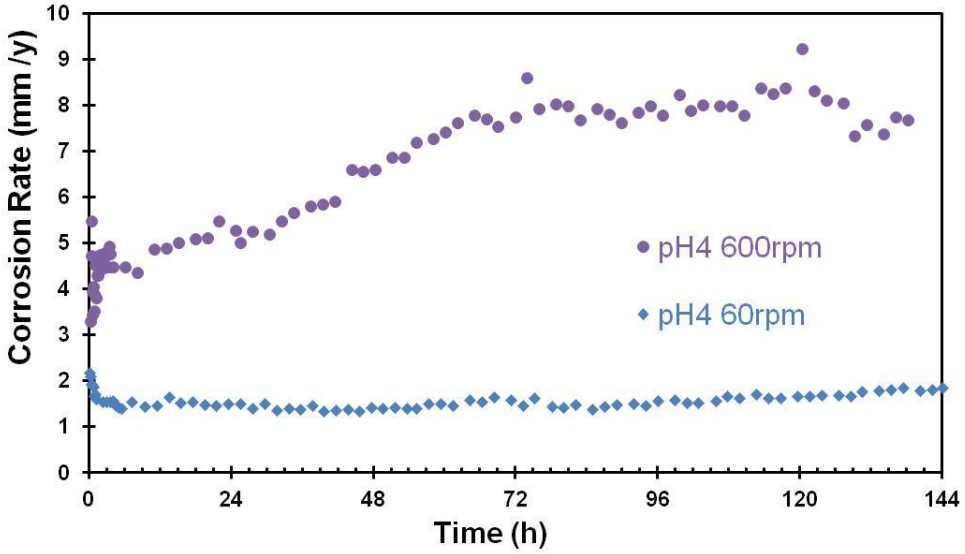

Figure 9. Effect of flow rate on corrosion rate change with time at pH 4.0, P_{total} = 1 bar, 10% H_2S /N_2 (0.05 bar H_2S), 80 °C.

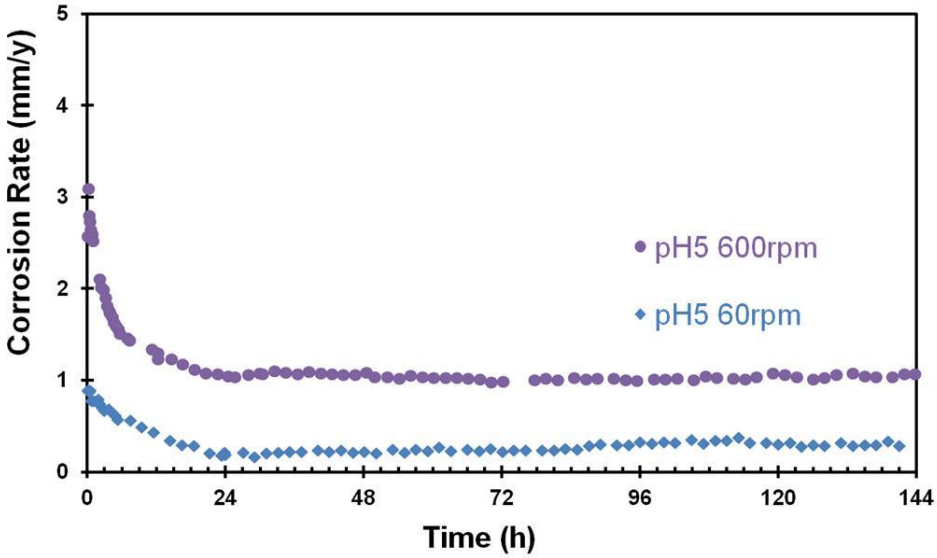

Figure 10. Effect of flow rate on corrosion rate change with time at pH 5.0, P_{total} = 1 bar, 10% H_2S /N_2 (0.05 bar H_2S), 80 °C.

Corrosion Product Layers

Figure 11 shows the effect of the flow on the surface morphology and cross section of the corrosion product layers at pH 4.0. At 600 rpm (high flow rate), the surface layer has a very open and porous structure and is detached from the steel surface, as shown in Figure 11 (a), (b). Consequently, the corrosion product layer cannot provide any protection against further corrosion. At 60 rpm (low flow rate), a more dense and adherent layer covering the steel surface with a thickness on average of about 20 µm was observed, which corresponds roughly to the thickness of steel loss (22 µm). The corrosion product layer was slightly more protective than that at 600 rpm (high flow rate), as the initial corrosion rate (2.2 mm/y) decreased to 1.5 mm/y corrosion rate.

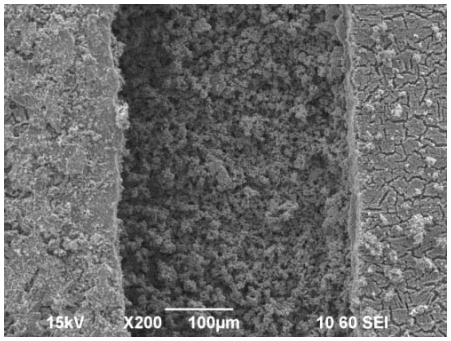

(a) SEM image of corrosion product layer at 600 rpm (high flow rate)

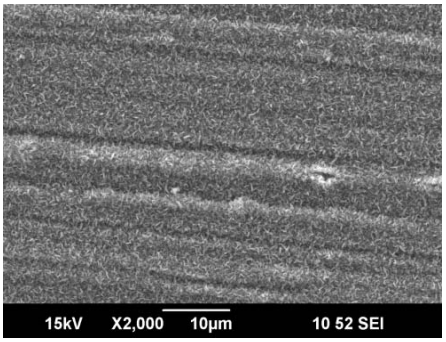

(c) SEM image of corrosion product layer at 60 rpm (low flow rate)

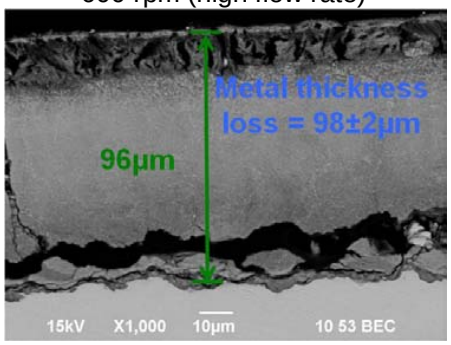

(b) Cross section of steel specimen with corrosion product layer at 600 rpm (high flow rate)

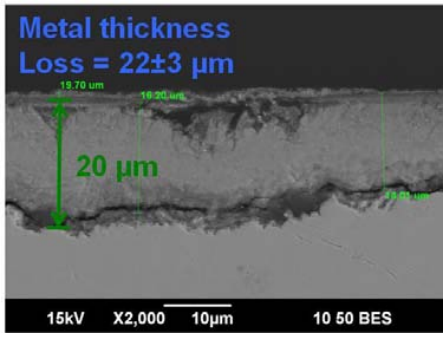

(d) Cross section of steel specimen with corrosion product layer at 60 rpm (low flow rate)

Figure 11. Effect of flow on the surface morphology and cross section of corrosion product layers at pH 4.0, P_{total} = 1 bar, 10% H_2S /N_2 (0.05 bar H_2S), 80 °C, 7 days exposure.

Figure 12 shows the effect of the flow on the surface morphology and cross section of the corrosion product layers at pH 5.0. The results have a similar dependence on flow rate as observed for pH 4.0. At a low flow rate (60 rpm), the rate of precipitation at the surface is much higher than the rate of corrosion (leading to a high SST) and tends to form a more protective corrosion product layer, which is dense and adherent to the steel surface, as Figure 12(d) shows.

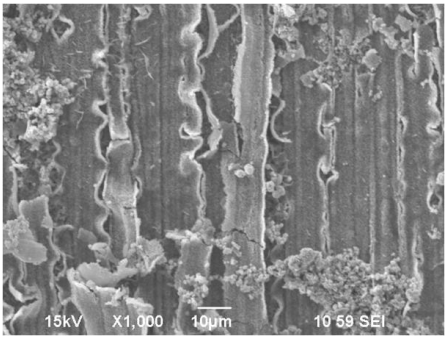

(a) SEM image of corrosion product layer at 600 rpm (high flow rate)

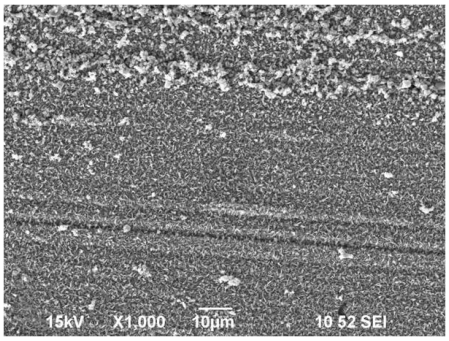

(c) SEM image of corrosion product layer at 60 rpm (low flow rate)

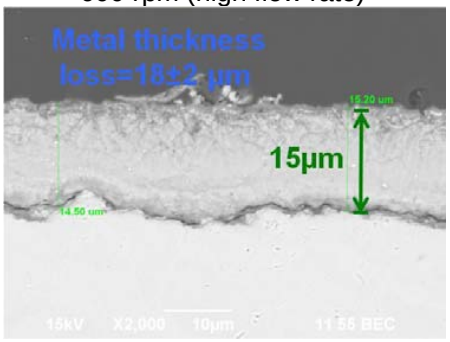

(b) Cross section of steel sample with corrosion product layer at 600 rpm (high flow rate)

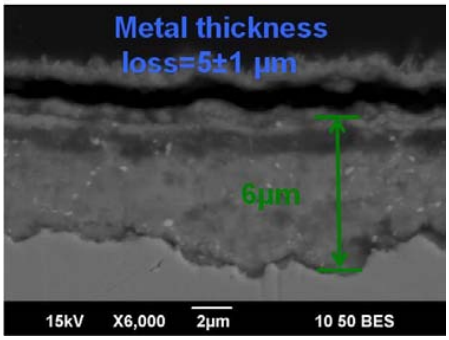

(d) Cross section of steel sample with corrosion product layer at 60 rpm (low flow rate)

Figure 12. Effect of flow on the surface morphology and cross section of corrosion product layers at pH 5.0, P_{total} = 1 bar, 10% H_2S /N_2 (0.05 bar H_2S), 80 °C, 7 days exposure.

Test series #3 - Temperature Effect

In the absence of any precipitation and corrosion product layer formation (i.e., at the initial stages of corrosion), temperature accelerates the kinetics of all the processes involved in a corroding system: electrochemical reactions, chemical reactions, transport processes, etc. Hence, the initial corrosion rate also increases with temperature as indicated in Figure 13.

When the formation of the corrosion product layer occurs by precipitation, it is known that increased temperature aids the iron sulfide layer formation by accelerating the kinetics of precipitation. At 25 °C the kinetics of iron sulfide precipitation is very much slower than that at 80 °C. Only a very porous layer formation can be detected at 25 °C, as shown in Figure 14 (c) and (d), which does not provide sufficient protection against corrosion (the corrosion rate is fairly constant from 0.4 mm/y to 0.3 mm/y). At 80 °C Figure 14 (a) and (b) show a thin, dense and adherent iron sulfide layer formed on the steel surface, which provides very good protection against corrosion, reducing the corrosion rate from 1.1 mm/y to 0.1 mm/y. In summary, higher temperatures make the initial corrosion rate higher, but make the final corrosion rate lower, which is shown in Figure 13.

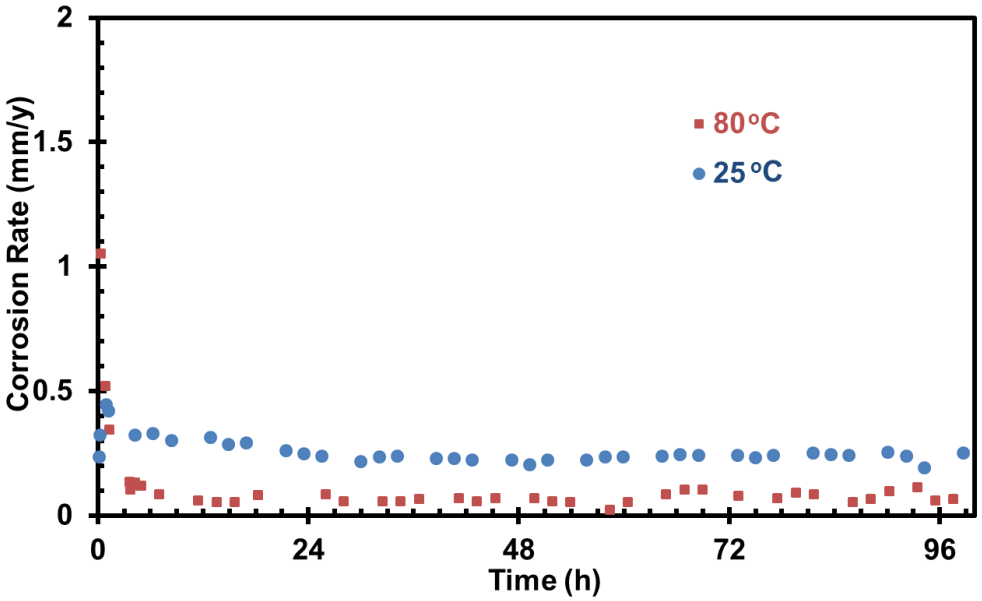

Figure 13. Effect of temperature on corrosion rate change with time at pH 6.0, P_{total} = 1 bar, 10% H_2S /N_2, 80 °C

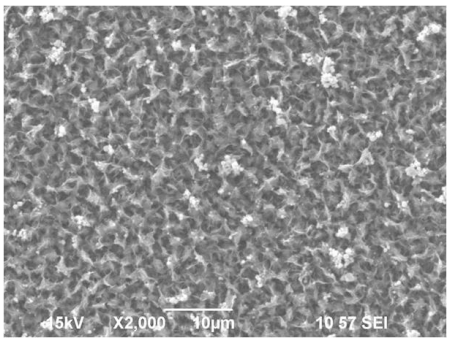

(a) SEM image of corrosion product layer at 80 °C (high temperature)

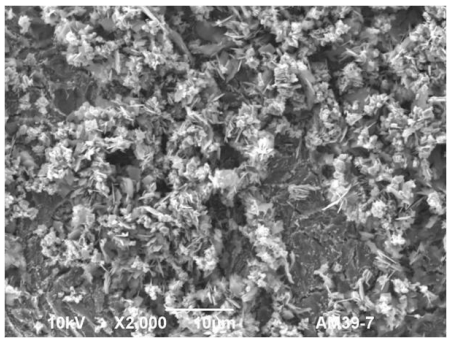

(c) SEM image of corrosion product layer at 25 °C (low temperature)

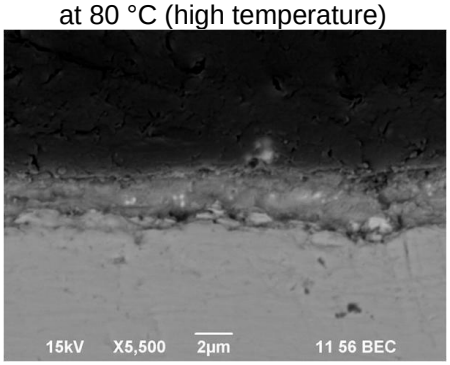

(b) Cross section of steel specimen with corrosion product layer at 80°C (high temperature)

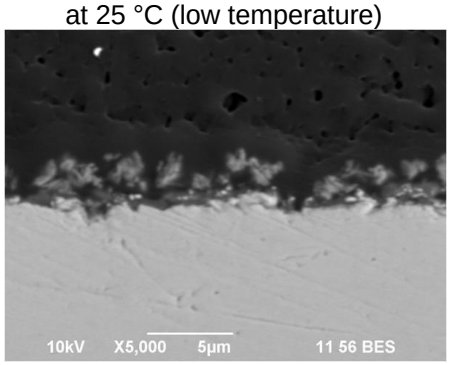

(d) Cross section of steel specimen with corrosion product layer at 25 °C (low temperature)

Figure 14. Effect of temperature on the surface morphology and cross section of corrosion product layers at pH 6.0, P_{total} = 1 bar, 10% H_2S /N_2, 80 °C, 4 days exposure.

Composition of corrosion product

EDS and XRD were used to characterize the composition of the corrosion product layer on the steel surface. XRD results show mackinawite is the dominant corrosion product except at pH 4.0. At pH 4.0, iron carbide is the dominant corrosion product after one day exposure, shown in Figure 15. Other iron sulfides such troilite and pyrrhotite appear at the end of the some tests, which is shown in Figure 16 as an example.

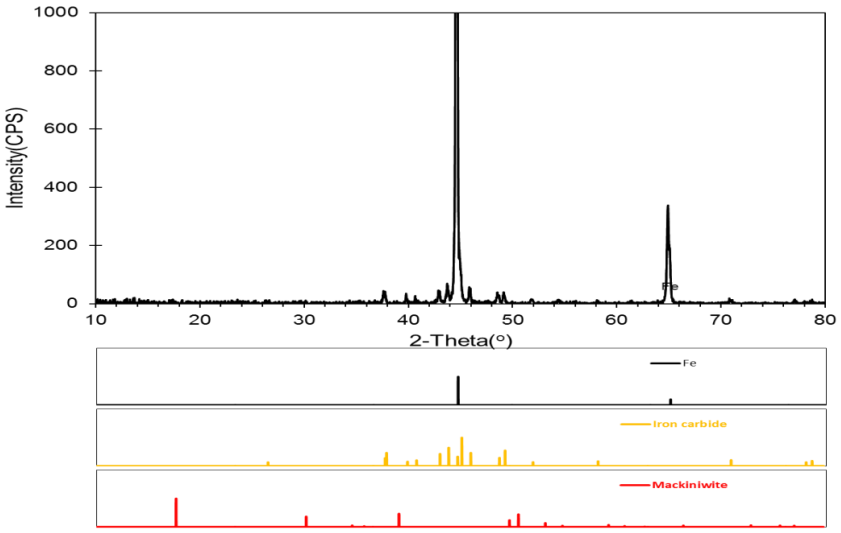

Figure 15. XRD analysis of surface corrosion products after 1 day corrosion, showing mostly FeC_3. Conditions: pH 4.0, 600rpm stirring rate, 80 °C, 1 wt% NaCl solution, 0.054 bar H_2S, balance N_2.

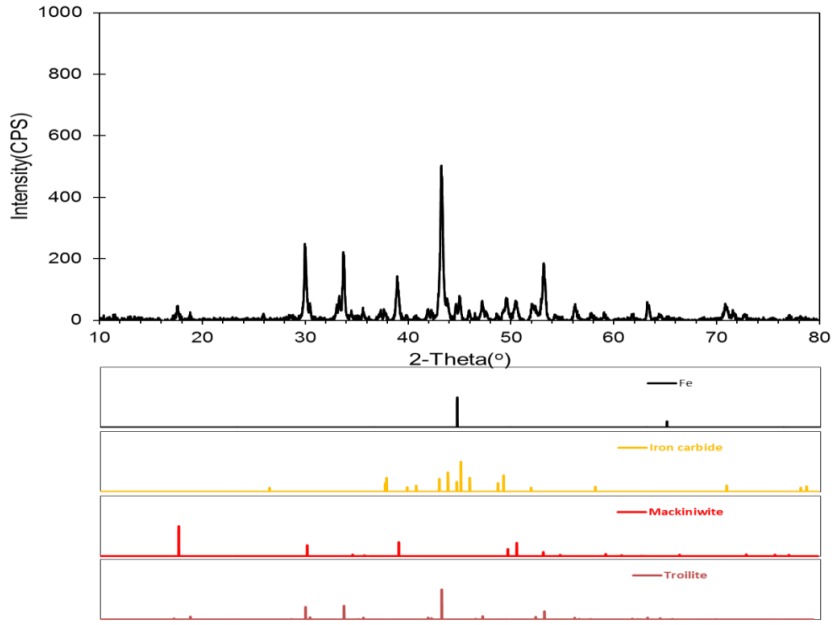

Figure 16. XRD analysis of surface corrosion products after 7 days corrosion, showing iron carbide, Mackinawite, Troilite. Conditions: pH 4.0, 600rpm stirring rate, 80 °C, 1 wt% NaCl solution, 0.054 bar H_2S, balance N_2.

CONLUSIONS

- A double layer structure of an iron sulfide layer formed in H_2S corrosion of mild steel as proposed by Sun *et al.*[4] was confirmed, which composed of a very thin inner film and a much thicker outer layer. However, the mechanism of formation and the role this layers play is not the same as originally described by Sun *et al.*[4].

- It is most likely that the very thin inner sulfide layer is formed by chemisorption. The chemically adsorbed sulfide layer slows down corrosion by affecting the charge transfer reaction kinetics, where both anodic and cathodic reactions are affected.

- The outer iron sulfide layer is formed by precipitation at the corroding steel surface and is a strong function of surface water chemistry.

- The protectiveness of the outer iron sulfide layer depends on the balance between iron sulfide precipitation which forms the layer and the corrosion which undermines it. This can lead to a variety of long-term corrosion outcomes depending on the environmental parameters such as temperature, pH, and flow rate.

- The protective iron sulfide corrosion product layer and low corrosion rate were observed at high pH, temperature and low flow rate due to high precipitation rate of a dense corrosion product layer.

- The present results also confirm that the concept of surface scaling tendency is a good indicator for assessing the likelihood of the formation of protective iron sulfide layers.

ACKNOWLEDGEMENTS

The authors would like to express sincere appreciation to the following industrial sponsors for their financial support and direction: BP, Champion Technologies, Chevron, Clariant Oil Services, ConocoPhilips, ENI S. P. A., ExxonMobil, Inpex Corporation, NALCO Energy Services, Occidental Petroleum Co., Petrobras, PETRONAS, PTT, Saudi Aramco, Total, TransCanada, MI-SWACO, HESS and WGIM. The authors also appreciate the help from the Center for Electrochemical Engineering Research, Department of Chemical and Biomolecular Engineering at Ohio University for XRD analysis. Last but not least, great thanks go to Cody Shafer for the assistance in constructing the figures of experimental set-up.

REFERENCES

1. Y. Zheng, B. Brown, and S. Nešić, “Electrochemical Study and Modeling of H_2S Corrosion of Mild Steel,” *Corrosion* 70 (2014): pp. 351–365.
2. Y. Zheng, J. Ning, B. Brown, and S. Nesic, “Electrochemical Model of Mild Steel Corrosion in a Mixed H_2S/CO_2 Aqueous Environment,” CORROSION/2014, paper no. 3907 (Houston, TX: NACE, 2014).
3. W. Sun, “Kinetics of Iron Carbonate and Iron Sulfide Scale Formation in Carbon Dioxide/hydrogen Sulfide Corrosion,” Ph.D. dissertation, Ohio University, 2006.
4. W. Sun and S. Nesic, “A Mechanistic Model of Uniform Hydrogen Sulfide/carbon Dioxide Corrosion of Mild Steel,” *Corrosion* 65 (2009): pp. 291–307.
5. S. Nesic and W. Sun, “Corrosion in Acid Gas Solutions,” Sheir’s Corrosion, 2nd edition, edited by J.A. Richardson et al., (Elsevier, 2010), pp. 1270–1298.
6. D. E. Jiang and E. A. Carter, “Adsorption, Diffusion, and Dissociation of H_2S on Fe(100) from First Principles,” *J. Phys. Chem. B* 108 (2004): pp. 19140–19145.
7. P. Marcus and E. Protopopoff, “Potential-pH Diagrams for Adsorbed Species: Application to Sulfur Adsorbed on Iron in Water at 25 °C and 300 °C,” *J. Electrochem. Soc.* 137 (1990): pp. 2709–2712.

8. J. Ning, Y. Zheng, D. Young, B. Brown, and S. Nešić, “Thermodynamic Study of Hydrogen Sulfide Corrosion of Mild Steel,” *Corrosion* 70 (2014): pp. 375–389.
9. ASTM G1.05, “Standard Practice for Preparing, Cleaning, and Evaluating Corrosion Test Specimens” (West Conshohocken, PA: ASTM, 2011), http://www.astm.org/Standards/G1.htm (May 8, 2014).
10. P. Marcus, Ed., *Corrosion Mechanisms in Theory and Practice*, 2nd Revised edition (New York, NY: Marcel Dekker Inc, 2002).
11. D. E. Jiang and E. A. Carter, “First Principles Study of H_2S Adsorption and Dissociation on Fe(110),” *Surf. Sci.* 583 (2005): pp. 60–68.
12. M. Volmer, M. Stratmann, and H. Viefhaus, “Electrochemical and Electron Spectroscopic Investigations of Iron Surfaces Modified with Thiols,” *Surf. Interface Anal.* 16 (1990): pp. 278–282.
13. Y.-S. Choi, S. Nesic, and S. Ling, “Effect of H_2S on the CO_2 Corrosion of Carbon Steel in Acidic Solutions,” *Electrochimica Acta* 56 (2011): pp. 1752–1760.
14. M. Volmer-Uebing and M. Stratmann, “A Surface Analytical and an Electrochemical Study of Iron Surfaces Modified by Thiols,” *Appl. Surf. Sci.* 55 (1992): pp. 19–35.
15. M. D. Lay, K. Varazo, and J. L. Stickney, “Formation of Sulfur Atomic Layers on Gold from Aqueous Solutions of Sulfide and Thiosulfate: Studies Using EC-STM, UHV-EC, and TLEC,” *Langmuir* 19 (2003): pp. 8416–8427.
16. E. Protopopoff and P. Marcus, “Effect of Chemisorbed Sulfur on the Electrochemical Hydrogen Adsorption and Recombination Reactions on Pt (111),” *J. Vac. Sci. Technol. Vac. Surf. Films* 5 (1987): pp. 944–947.
17. M. Rohwerder and M. Stratmann, “Surface Modification by Ordered Monolayers: New Ways of Protecting Materials against Corrosion,” *MRS Bull.* 24 (1999): pp. 43–47.
18. A. Srhiri, M. Etman, and F. Dabosi, “Thiol Compounds as Corrosion Inhibitors of Carbon Steel (XC 38) in Sodium Chloride Medium,” *Mater. Corros.* 43 (1992): pp. 406–414.
19. J. L. Crolet, N. Thevenot, and A. Dugstad, “Role of Free Acetic Acid on the CO_2 Corrosion of Steels,” CORROSION/99, paper no. 99024 (Houston TX: NACE, 1999).
20. Y. Sun, K. George, and S. Nesic, “The Effect of Cl^- and Acetic Acid on Localized CO_2 Corrosion in Wet Gas Flow,” CORROSION/2003, paper no. 03327 (Houston, TX: NACE, 2003).
21. E. Gulbrandsen and K. Bilkova, “Solution Chemistry Effects on Corrosion of Carbon Steels in Presence of CO_2 and Acetic Acid,” CORROSION/2006, paper no. 06364 (Houston, TX: NACE, 2006).
22. N. Sato, *Electrochemistry at Metal and Semiconductor Electrodes* (Amsterdam. New York: Elsevier, 1998).
23. J. Ning, B. Brown, and S. Nesic, “Verification of Pourbaix Diagrams for the H_2S-H_2O-Fe System at 25 ^oC,” ICMT Ohio University Advisory Board Meeting, (March, 2012).
24. F. Farelas, B. Brown, and S. Nesic, “Iron Carbide and Its Influence on the Formation of Protective Iron Carbonate in CO_2 Corrosion of Mild Steel,” CORROSION/2013, paper no. 02291 (Houston TX: NACE, 2013).
25. J. L. Crolet, N. Thevenot, and S. Nesic, “Role of Conductive Corrosion Products in the Protectiveness of Corrosion Layers,” *Corrosion* 54 (1998): pp. 194–203.
26. S. Nesic, A. Stangeland, M. Nordsveen, and R. Nyborg, “A Mechanistic Model for Carbon Dioxide Corrosion of Mild Steel in the Presence of Protective Iron Carbonate Films Part 2: A Numerical Experiment,” *Corrosion* 59 (2003): pp. 489–497.